

Analysis of field-free region formed by parametric positioning of a magnet pair for targeted magnetic hyperthermia

Serhat Küçükdermenci^{1, *}

¹*Dept. of Electrical and Electronics Engineering, Balikesir University,
Balikesir, Turkey*

**Corresponding author: kucukdermenci@balikesir.edu.tr*

Abstract

One of the challenges in using magnetic fluid hyperthermia in practical applications is the limited control of magnetic nanoparticle oscillations. In this study, we investigated how the form and location of a static magnetic field-free region can be modified by the symmetrical and asymmetrical positioning of a magnet pair. The gradient patterns in the workspace were estimated using a finite element method simulation. On an experiment platform, measurements were taken using a point probe. It has been demonstrated that parametric changes in distance and angle allow changing of the form and location of the field-free region. Field-free regions can shrink and have shapes similar to a line or point. The focus of the field-free region can be directed to various parts of the target object. The mapping of gradient patterns formed by a magnet pair for the use of targeted magnetic fluid hyperthermia is described for the first time in this paper. Furthermore, the findings highlight the significance of the fit between the target objects and the created gradient models.

Keywords: Cancer treatments; field-free region; gradient pattern; magnetic fluid hyperthermia; permanent magnet.

1. Introduction

Magnetic fluid hyperthermia (MFH) is a medical procedure in which cancerous cells are brought to a temperature between 42-46 °C with magnetic nanoparticles (MNPs) (Deatsch & Evans, 2014). When MNPs are exposed to an alternating magnetic field (AMF), the magnetic energy is converted into heat energy with the oscillating movement. Cancerous cells lose their effectiveness with the high temperature in the environment. Inversely, healthy cells are more resistant to heat than cancer cells. The heat generating capacity of MNPs is defined as the specific absorption rate (SAR) and it is expressed by Equation 1.

$$SAR = c \frac{V_s}{m_{MNP}} \times \frac{dT}{dt} \quad (1)$$

Here, c is the specific heat capacity of the medium, V_S is the volume of the sample, m_{MNP} is the mass of the MNPs, and dT/dt is the time derivative of the temperature difference.

The heat production of MNPs by the AMF effect is explained by the relaxation losses. The deflection motion of MNP moments is defined as Neel relaxation. In Brownian relaxation, MNPs interact with the medium fluid and make a mechanical motion. The Neel and Brownian characteristic relaxation times are expressed as τ_N and τ_B , respectively. The effective relaxation time (τ_{eff}) is given by Equation 2.

$$\tau_{eff} = (\tau_B \cdot \tau_N) / (\tau_B + \tau_N) \quad (2)$$

One of the models describing the volumetric power density emitted by MNPs exposed to AMF is the Rosensweig model and it is expressed by Equation 3.

$$P = \pi \mu_0 \chi_0 H_{ac}^2 f \frac{\omega \tau}{1 + (\omega \tau)^2} [W / m^3] \quad (3)$$

Here, χ_0 is magnetic susceptibility, H_{ac} and f are AMF amplitude and frequency, τ is effective relaxation time and ω is angular frequency, respectively.

The typical problem in MFH applications is the difficulty of localizing the heat to the tumor without damaging the healthy tissues. Because there is a tendency for MNPs to migrate from the tumor site to healthy tissues during MFH tests. There are theoretical and experiment studies (Dhavalikar & Rinaldi, 2016), (Cantillon-Murphy *et al.*, 2010) showing that MNP behaviors under the influence of AMF can be changed by adding static magnetic field (SMF). SMF sources are positioned such that the SMF vectors bend each other (see Figure 1) and field-free region (FFR) occurs in the workspace (WS). MNPs remaining in FFR can oscillate freely under the influence of AMF. MNPs in the SMF are either restricted or completely blocked.

Among the studies on MFH, Tasci *et al.* (Tasci *et al.*, 2009) showed that the MNP temperature rise can be controlled with their proposed method. The SMF source made with DC coils is positioned on both sides of the AMF generating coil in their study. Lu *et al.*, 2020 used magnets to focus the heat on a specific area. This system is capable of performing magnetic particle imaging and MFH operations (Lu *et al.*, 2020). Ma *et al.* (Ma *et al.*, 2015) used Neodymium Iron Boron (NdFeB) magnets. It was reported that MNP samples remaining within the FFR effectively generate heat and the SAR value of MNPs is limited in the SMF. GP mapping has not been studied in detail in any of these studies. The mapping of GPs produced by a magnet pair (MP) for the use of targeted MFH is discussed for the first time in this study.

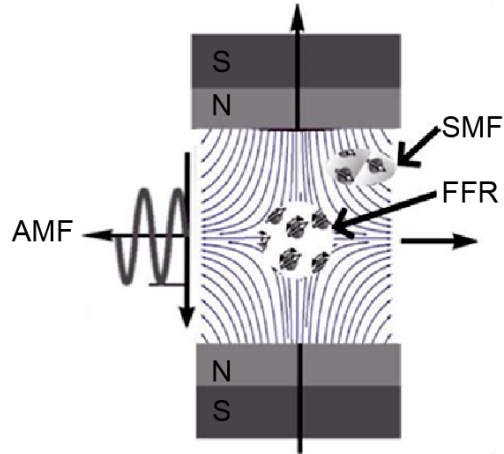


Fig. 1. Schematic representation of FFR.

2. Materials and methods

Literature comparison of WSs and target objects (TOs) are shown in Table 1. WSs are generally inner volume of helical shaped work-coil. Ferrofluid containing test tubes and regional tumor masses of small animals can be considered as the TO.

Table 1. Workspace and target object properties.

Properties of the WS	Properties of the TO	Ref.
Radius of the coil ≈ 5 cm, Cross-section area of WS ≈ 78.5 cm ²	One test-tube located in the center of the coil, the radius of the tube, $r \approx 0.5$ cm, Target area ≈ 0.785 cm ²	(Bauer <i>et al.</i> , 2016)
Radius ≈ 2 cm, height ≈ 6 cm, Cross-section area of WS ≈ 24 cm ²	Spherical plastic cups, $r \approx 0.2$ cm, target area ≈ 0.126 cm ²	(Tasci <i>et al.</i> , 2009)
Coil diameter = 3 cm	Two phantoms stay close to the heating region of the coil (20mm).	(Ma <i>et al.</i> , 2015)
Coil with a diameter = 3 cm,	Tube diameter = 8 mm, target area ≈ 0.502 cm ²	(Murase <i>et al.</i> , 2013)
Solenoid coil diameter = 4 cm, length = 10 cm. Cross-section area of WS ≈ 40 cm ²	Spherical core with a radius of 4.9 mm	(Zhao <i>et al.</i> , 2012)
90 mm diameter circle and a square of 56 x 56 mm ² can be fitted into it.	TO can be small test tube array, long test tube or a small test animal	Proposed study

Small test tubes (see Figure 2a) or a long test tube containing MNP can be TO for in vitro tests. A long test tube may have a length of 47.5 mm and an outer diameter of 9.6 mm (labeled with letters *A* and *B* in Figure 2b). If it is placed horizontally, the FFR can be applied to some parts of the tube. If TO is the tumor mass in the small animal, it can be in the shape of line-like or point-like geometries as shown with the letters *L* and *S* (see Figure 2c).

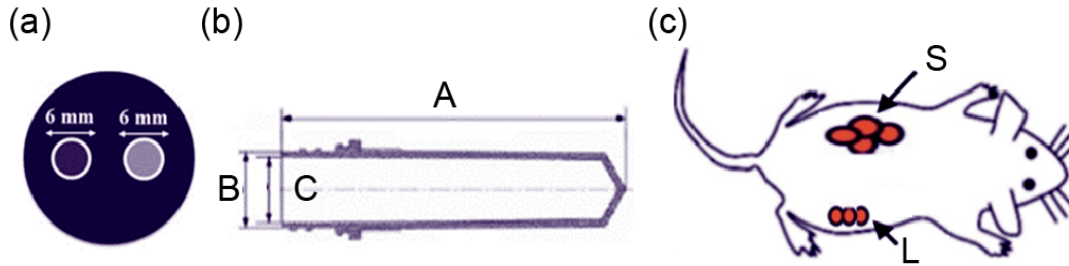


Fig. 2. Schematic representation of TOs (a) small tube, (b) long tube, (c) test animal.

In bioelectromagnetic applications, either current fed electromagnets (Ristic-Djurovic *et al.*, 2018) or permanent magnets (Ren *et al.*, 2019) are preferred as SMF sources. However, coils need power supplies and sometimes chiller. This makes experiment setup more complex and expensive. NdFeB magnets produce stronger SMF compared to coils (Mahadi *et al.*, 2003). Experiment setups containing magnets are less complex and cost-effective than coils.

Due to the properties mentioned above it was decided to use the following materials and methods. NdFeB magnets were preferred in this study. NdFeB magnets with volume of $50 \times 10 \times 20 \text{ mm}^3$ were used. N54 has relative magnet permeability and B_r of 1.05 T and 1.47 T, respectively. (d_1, d_2) are the distances from the center point of magnets to the origin and (θ_1, θ_2) are angles of magnets referencing the x-axis. Six cases were chosen to investigate effect of magnet positions on FFR (see Table 2).

Table 2. Magnet positions and angles.

(θ_1, θ_2) degrees	(d_1, d_2) mm	Case
(180, 0)	(-70, 70)	1
(180, 0)	(-60, 60)	2
(180, 0)	(-70, 60)	3
(180, 0)	(-80, 60)	4
(225, 45)	(-60, 60)	5
(197, -17)	(-60, 60)	6

2.1 Simulation medium

A multiphysics simulation software (COMSOL® Multiphysics, COMSOL AB, Stockholm, Sweden) was used for GP modeling. Simulation medium consists of source magnets and TO. The TO is a cylinder has a radius of 28 mm and a height of 56 mm as shown in Figure 3a. This cylinder could be a representative model for a work area. Test tube or a small animal can be placed in this space for in vitro or in vivo applications.

2.2 Experiment setup

3D-printed experiment setup consists of magnets, holders, arms and center platform (see Figure 3b). Magnets are placed inside the holders. The distances and angles can be changed gradually by

the help of arms. Holders, arms and center platform are connected together. Center platform keeps all system aligned, and its center room was used for measuring. This room is a 90 mm diameter circle and a square of $56 \times 56 \text{ mm}^2$ can be fitted into it. WP and TO comparison can be found in Table 1. Technical drawings of each part and information of 3D printing process can be found as a file in supplementary materials.

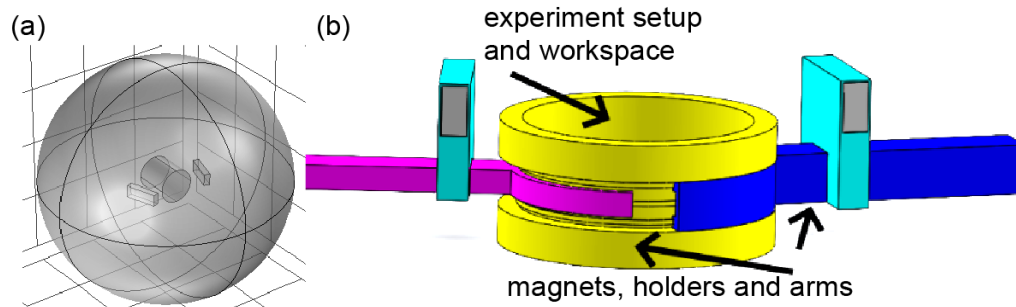


Fig. 3. (a) simulation medium, (b) experiment setup.

3. Results and discussion

3.1 Simulation results

Color maps and arrow representations of flux lines for different parametric values are shown in Figure 4 a-f, respectively.

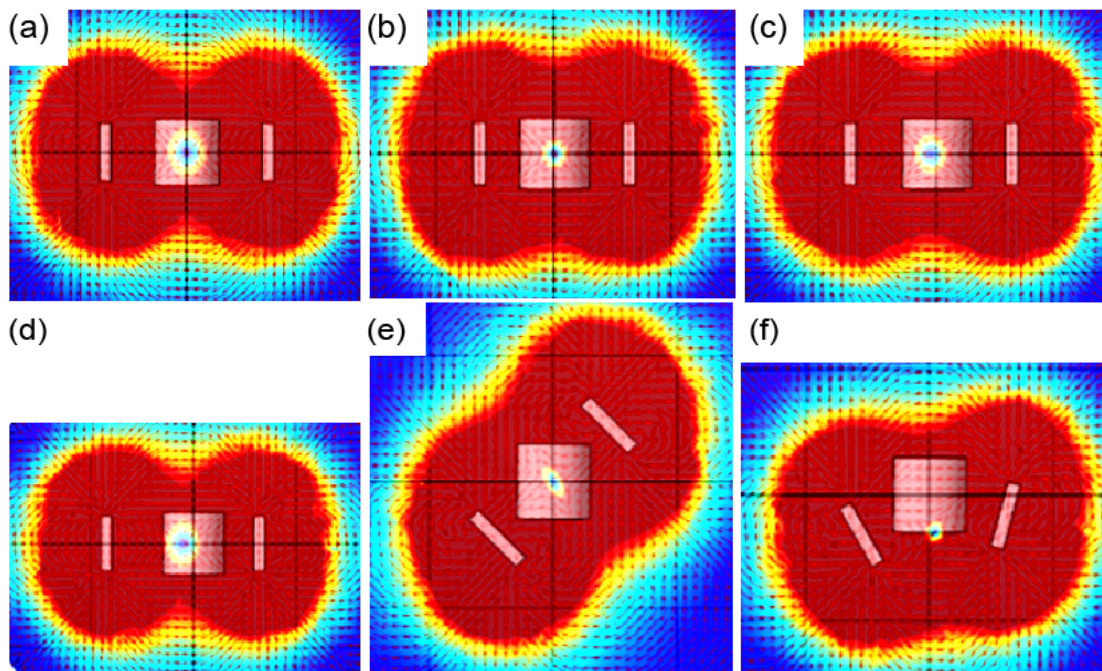


Fig. 4. GPs for (a) Case 1, (b) Case 2, (c) Case 3, (d) Case 4, (e) Case 5 and (f) Case 6.

For the linear symmetric cases (Case 1-2), it is found that the form of the FFR can shrink and focus in the center. For the linear asymmetric cases (Case 3-4), it is observed that FFR focus can be shifted and its form can be manipulated. FFR can be directed to different parts of the TO by using angular symmetric/asymmetric cases. From Case 5 to Case 6 the focus of FFR can be moved from the center point to the lower mid part of the TO. And its shape changes from a diagonal line form to a point-like form.

Conditions of MFH experiments in the literature vary widely. For example, AMF intensity can range from 0.8 to 115 kA/m (Vilas-Boas *et al.*, 2020). So the limit value of SMF can be selected as 20 G (≈ 1.6 kA/m). Contour lines are drawn and areas below 20 G are accepted as FFR (see Figure 5). FFR ($B \leq 20$ G) can be considered as ellipse. Semi-major axis a and semi-minor axis b of FFRs are measured. (a, b) are (2.15, 1.45), (1.15, 0.9), (1.45, 1.05) and (2.15, 1.3) cm for Case 1-4, respectively. It is found that if magnets come closer symmetrically, FFR can be focused into a very small area. (a, b) are (1.3, 0.55) and (1, 0.75) cm for Case 5 and Case 6, respectively. And the FFR can be in the form of diagonal line-like or point-like form for these cases. The equation $A = \pi ab$ gives the area of the ellipse. Area calculations were done for all cases. Surface areas are 9.79, 3.25, 4.78, 8.78, 2.25 and 2.36 cm² for Case 1-6, respectively. These surface areas can be suitable for TOs like small test tubes, long test tube or small test animal.

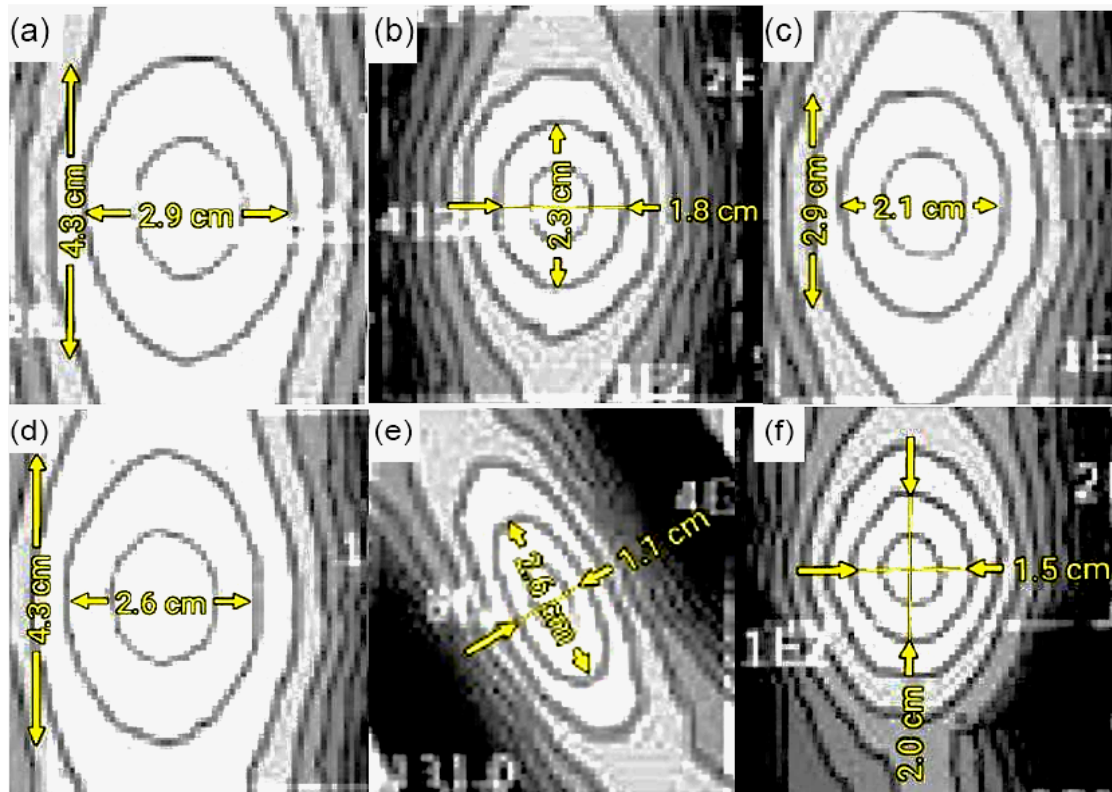


Fig. 5. Axis measurements of FFR for a) Case 1, b) Case 2, c) Case 3, d) Case 4, e) Case 5 and f) Case 6.

Total 49 measurement points were determined on the x and y axes with 8 mm intervals from -24 mm to 24 mm in WS (see Figure 6). Point probe measurements (PPMs) of SMF for simulation environment are generated for all cases. Related tables can be found as a file in the supplementary material.

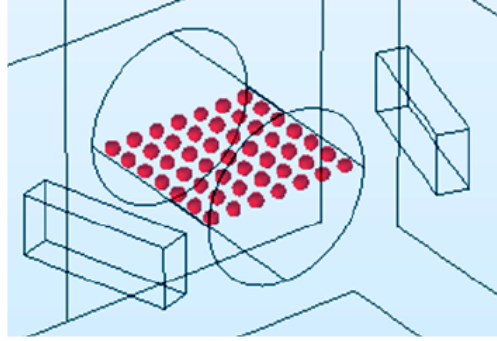


Fig. 6. Probe positions in the simulation setup.

3.2 Experiment setup results

PPMs were made at the same probe positions as in the simulation. Magnetic flux measurements in the x and y directions (B_x and B_y) were taken for all cases with WT10A commercial magnetic flux meter. The magnitude of vector B for every point was calculated by Equation 4.

$$B = \sqrt{B_x^2 + B_y^2} \quad (4)$$

Measurements were repeated four times in a row and the average values were transferred to Table 3. The number of points forming the FFR (red colored regions in Table 3, $B \leq 20$ G) are 5, 1, 2, 4, 1, and 1 for Case 1-6, respectively. It is seen that PPMs in the experiment setup also give information about the position and flux density levels of the FFRs.

Table 3. Point probe measurements.

		Case 1						Case 2						Case 3								
		x-axis prob position (mm)						x-axis prob position (mm)						x-axis prob position (mm)								
B (G)		-24	-16	-8	0	8	16	24	-24	-16	-8	0	8	16	24	-24	-16	-8	0	8	16	24
y axis probe	40	92	65	49	48	48	65	92	163	112	83	74	83	105	164	96	68	60	59	74	99	165
	30	82	57	42	33	39	55	87	142	99	66	54	65	86	151	79	59	43	48	60	84	149
	8	74	46	25	17	25	47	74	125	76	45	33	41	77	127	69	41	26	31	43	78	128
	0	71	42	19	2	18	43	76	125	68	36	3	35	68	133	72	37	11	17	46	79	137
	-8	74	50	27	17	30	43	73	130	79	44	32	47	70	129	70	43	28	30	50	79	132
	-16	84	61	38	34	41	59	82	144	102	66	56	63	97	138	82	61	46	46	60	98	141
	-24	94	64	54	46	48	63	92	165	106	84	72	82	108	161	94	70	61	61	75	105	160
		Case 4						Case 5						Case 6								
		x-axis prob position (mm)						x-axis prob position (mm)						x-axis prob position (mm)								
B (G)		-24	-16	-8	0	8	16	24	-24	-16	-8	0	8	16	24	-24	-16	-8	0	8	16	24
y axis probe	40	62	48	49	51	68	99	156	78	72	81	99	165	271	485	137	102	87	82	88	103	130
	30	49	36	37	44	61	87	146	86	72	55	68	119	185	321	158	119	94	91	94	113	153
	8	41	26	18	7	30	52	83	133	110	76	38	39	66	152	208	166	120	91	84	##	126
	0	40	14	7	26	47	79	141	165	97	49	6	49	110	164	170	109	86	82	86	122	180
	-8	43	27	18	31	53	80	137	217	146	74	34	38	74	108	163	100	68	57	67	103	176
	-16	51	37	36	41	60	96	138	324	202	120	69	53	67	89	173	92	46	27	49	94	166
	-24	61	49	48	54	71	105	162	458	281	167	95	72	72	83	182	91	44	16	42	91	170

3.3 Discussion

Small deviations of PPMs between simulation medium and experiment setup may have different reasons. Magnets are identical in simulation medium but in real life they may not be exactly the same. Commercial flux meter measurements were done with hand and probe alignments can't be perfect as in the simulation. Some gaps should be added to the 3D printed objects for assembly. For example, the magnet edges should be set to 10 and 20 mm, while the room edges in the holder should be set to 10.3 and 20.3 mm. The gaps were left for assembly and the 3D printouts could be different from the ideal dimensions in the technical drawing. This can lead to inevitable alignment and measurement differences (see supplementary material).

A brief literature comparison of MFH studies including SMF sources is presented in Table 4. It is seen that both DC current fed coils and magnets can be used as SMF sources. The opposite or same SMF poles can face each other. Topics like parametrization of linear distance and angle, major and minor axis measurements and area calculations of FFR, PPMs and GP mapping have not been studied in detail in any of these studies. This proposed study addresses these topics.

Table 4. Comparison of MFH studies.

Reference	SMF source / Flux direction	Parametrization of linear distance and angle	GP mapping	FFR measurements
(Bauer <i>et al.</i> , 2016)	Magnet Single magnet, MP / same dir.	-	-	-
(Tasci <i>et al.</i> , 2009)	DC fed coil A pair / opposite dir.	-	-	-
(Ma <i>et al.</i> , 2015)	Magnet A pair / opposite and same dir.	-	-	-
(Murase <i>et al.</i> , 2013)	DC fed coil A pair / same dir.	-	-	-
(Zhao <i>et al.</i> , 2012)	DC fed coil A pair / same dir.	-	-	-
Proposed study	Magnets A pair / opposite direction	The symmetrical and asymmetrical situations of distance and angle are examined.	PPMs are taken in WS for FFR investigations.	FFR major and minor axis measurements and area calculations are done.

4. Conclusions

In this study, GP mapping produced by parametric position changes of a MP for using in targeted MFH tests was investigated for the first time. It is found that symmetric and asymmetric displacements of a MP can manipulate FFR form (changes its shape to surface, line and point like forms) and location (can be focused to center or edge of the TO). FFR structures were analyzed with color maps and arrow representations, axis measurements and area calculations from contour representations, PPMs and GP mappings. Considering cross-sectional region of TO and the WS quite suitable choices can be made for in vitro and in vivo MFH experiments among the GPs

mapped in this study. For in vitro tests, FFR can be applied to test tubes in periodic array or a long tube with horizontal positioning. For MFH test with small animals, FFR and target tissue overlap can be achieved by appropriate placement of the SMF source and/or TO. The utilized system in this study could be used in real scenario if the specific conditions of each experiment are taken into account.

The obtained results provide data for in vitro and in vivo MFH tests performed prior to clinical trials. With the help of GP mapping, suitable FFRs for different tumor geometries can be determined. The ability to ablate a tumor of any possible geometry by moving the FFR over the tumor is important for future studies. This highlights the importance of adapting the position and shape of the FFR in MFH applications. In the future, designs may be considered to focus FFR with highly sensitive robotic devices for each patient's unique individual conditions.

Supplementary material

The PPMs in simulation medium, technical drawings of each part and information of 3D printing process for experiment setup are available online at https://docs.google.com/document/d/1-ZgJM6A52fsg9gH_Kx6iLBgRIwojSAtX.

References

- Bauer, L. M., Situ, S. F., Griswold, M. A., & Samia, A. C. S. (2016)** High-performance iron oxide nanoparticles for magnetic particle imaging-guided hyperthermia (hMPI). *Nanoscale*, 8(24), 12162–12169.
- Cantillon-Murphy, P., Wald, L. L., Zahn, M., & Adalsteinsson, E. (2010)** Proposing magnetic nanoparticle hyperthermia in low-field MRI. *Concepts in Magnetic Resonance Part A: Bridging Education and Research*, 36(1), 36–47.
- Deatsch, A. E., & Evans, B. A. (2014)** Heating efficiency in magnetic nanoparticle hyperthermia. *Journal of Magnetism and Magnetic Materials*, 354, 163–172.
- Dhavalikar, R., & Rinaldi, C. (2016)** Theoretical predictions for spatially-focused heating of magnetic nanoparticles guided by magnetic particle imaging field gradients. *Journal of Magnetism and Magnetic Materials*, 419, 267–273.
- Lu, Y., Rivera-Rodriguez, A., Tay, Z. W., Hensley, D., Fung, K. L. B., Colson, C., Saayujya, C., Huynh, Q., Kabuli, L., Fellows, B., Chandrasekharan, P., Rinaldi, C., & Conolly, S. (2020)** Combining magnetic particle imaging and magnetic fluid hyperthermia for localized and image-guided treatment. *International Journal of Hyperthermia*, 37(3), 141–154.
- Ma, M., Zhang, Y., Shen, X., Xie, J., Li, Y., & Gu, N. (2015)** Targeted inductive heating of nanomagnets by a combination of alternating current (AC) and static magnetic fields. *Nano Research*, 8(2), 600–610.

Mahadi, W. N. L. W., Adi, S. R., & Nor, K. M. (2003) Application of the rare earth permanent magnet in linear generator driven by an internal combustion engine. National Power Engineering Conference, PECon 2003 - Proceedings, 256–261.

Murase, K., Takata, H., Takeuchi, Y., & Saito, S. (2013) Control of the temperature rise in magnetic hyperthermia with use of an external static magnetic field. *Physica Medica*, 29(6), 624–630.

Ren, Z. H., Mu, W. C., & Huang, S. Y. (2019) Design and Optimization of a Ring-Pair Permanent Magnet Array for Head Imaging in a Low-Field Portable MRI System. *IEEE Transactions on Magnetics*, 55(1), 1–8.

Ristic-Djurovic, J. L., Gajic, S. S., Ilic, A. Z., Romcevic, N., Djordjevich, D. M., De Luka, S. R., Trbovich, A. M., Jokic, V. S., & Cirkovic, S. (2018) Design and Optimization of Electromagnets for Biomedical Experiments With Static Magnetic and ELF Electromagnetic Fields. *IEEE Transactions on Industrial Electronics*, 65(6), 4991–5000.

Tasci, T. O., Vargel, I., Arat, A., Guzel, E., Korkusuz, P., & Atalar, E. (2009) Focused RF hyperthermia using magnetic fluids. *Medical Physics*, 36(5), 1906–1912.

Vilas-Boas, V., Carvalho, F., & Espiña, B. (2020) Magnetic hyperthermia for cancer treatment: Main parameters affecting the outcome of in vitro and in vivo studies. *Molecules*, 25(12).

Zhao, Q., Wang, L., Cheng, R., Mao, L., Arnold, R. D., Howerth, E. W., Chen, Z. G., & Platt, S. (2012) Magnetic nanoparticle-based hyperthermia for head & neck cancer in mouse models. *Theranostics*, 2(1), 113–121.

Submitted: 06/09/2021

Revised: 20/11/2021

Accepted: 22/11/2021

DOI: 10.48129/kjs.16097